JOM, Vol. 71, No. 6, 2019
https://doi.org/10.1007/s11837-019-03438-3

TECHNICAL ARTICLE

Synthesis of 3D Hierarchical Rose-Like Bi_2WO_6 Superstructure with Enhanced Visible-Light-Induced Photocatalytic Performance

YANAN WANG,[1] YIQING ZENG,[1] SHULE ZHANG,[1,2] and QIN ZHONG[1,3]

1.—School of Chemical Engineering, Nanjing University of Science and Technology, Nanjing 210094, People's Republic of China. 2.—e-mail: shulezhang@163.com. 3.—e-mail: zq304@njust.edu.cn

A novel three-dimensional (3D) hierarchical rose-like Bi_2WO_6 (BWR) superstructure for use as an efficient visible-driven photocatalyst has been fabricated using a facile template-free hydrothermal strategy to integrate sequentially two-dimensional (2D) nanoplates into the 3D hierarchical structure. The formation mechanism was briefly analyzed. The 3D hierarchical superstructure facilitated migration and separation of photogenerated charge carriers due to the stacked hierarchical subunits, increased surface area for pollution adsorption, and more exposed active sites for surface redox catalysis. Benefiting from its excellent structural features, the BWR exhibited enhanced performance for photodegradation of RhB and photooxidation of NO under visible-light irradiation compared with irregular Bi_2WO_6. In addition, a trapping experiment was conducted to reveal which active species are involved in the photodegradation of RhB.

INTRODUCTION

In the last decade, semiconductor photocatalytic technology has been considered to represent a promising avenue to address the energy crisis and environmental pollution through the use of plentiful solar energy.[1,2] Use of semiconductors is one of the most important factors in such photoreactions. Consequently, exploitation of high-performance photocatalysts has become one of the most attractive research hotspots in the photocatalysis field. To date, the semiconductor TiO_2 has attracted much interest as a promising photocatalyst because of its nonpoisonous nature, low cost, and excellent stability.[3–5] Nonetheless, the wide bandgap of TiO_2 (3.2 eV) means that it can only respond to ultraviolet (UV) light (representing less than 4% of the solar light), limiting its practical applications.[6] Therefore, much effort has been made to improve the visible-light response of TiO_2, e.g., by doping with N, C, or S.[7–9] However, such doped TiO_2 materials still show poor absorption of solar light and photocatalytic performance. It is thus of great significance to develop more effective and convenient ways to synthesize other visible-light catalysts to further meet the requirements of environmental pollutant treatment.

Bi_2WO_6, the simplest Aurivillius oxide with a layered structure, possesses attractive physical properties, such as oxide anion conduction, nonlinear dielectric susceptibility, ferroelectric piezoelectricity, and pyroelectricity.[10–12] In particular, Bi_2WO_6 has attracted considerable attention as a visible-light-driven photocatalyst because of its suitable bandgap of 2.75 eV and high stability.[12–14] However, the photocatalytic performance of bulk Bi_2WO_6 is limited by its relatively poor adsorption performance and the short lifetime of the photoinduced electron–hole pairs. Previous studies have investigated whether the photocatalytic performance of Bi_2WO_6 can be improved by adjusting its morphology, size, and structural features.[12,15,16]

Recently, three-dimensional (3D) superstructures assembled from one-dimensional (1D) or two-dimensional (2D) nanostructures have attracted great interest due to their unique morphology and surface structure, which is considered as a key step in implementing functional systems.[17,18] It has

(Published online March 19, 2019)

gradually been determined that tailoring of the morphology is one of the most promising approaches to improve the properties and applications of photocatalysts.[19] Hence, much effort has been devoted to synthesis of Bi_2WO_6 with different morphologies, including nanoplates,[20] nanoparticles,[21] nest-like superstructures,[22] flower-like superstructures,[23] and microspheres,[24] all of which exhibited enhanced photocatalytic performance. However, to date, few reports have focused on synthesis and characterization of rose-like Bi_2WO_6 superstructures. We report herein a surfactant-free hydrothermal method to obtain single-crystal 3D hierarchical rose-like Bi_2WO_6 superstructure by facilely changing the pH value. The relationship between the photocatalytic performance and the new morphology of Bi_2WO_6 was then investigated.

EXPERIMENTAL PROCEDURES

Preparation of Materials

Synthesis of 3D Rose-Like Bi_2WO_6 Photocatalyst

$Bi(NO_3)_3{\cdot}5H_2O$ (2.5 mmol) was added into 50 mL aqueous solution with stirring at 40°C. Then, 1.25 mmol $Na_2WO_4{\cdot}2H_2O$ mixed in 50 mL deionized water was added into the above solution of $Bi(NO_3)_3$ with vigorous stirring. Thereafter, $NH_3{\cdot}H_2O$ was slowly dropped into the mixture solution under vigorous stirring for 6 h. Then, the mixture was maintained in a 200-mL Teflon-lined autoclave at 200°C for 16 h. After cooling to room temperature, the precipitate was collected by centrifugation with water several times. Finally, the samples were dried in air at 60°C. The abovementioned experimental conditions were also followed to prepare irregular Bi_2WO_6 photocatalysts, not sealed and maintained with a Teflon-lined autoclave, but calcinated at 550°C for 4 h after centrifugation and drying.

Characterization

The structure of the samples was characterized by x-ray diffraction (XRD) analysis (Cu K, Purkinjie XD-3). Ultraviolet–visible (UV–Vis) diffuse reflectance spectroscopy (DRS) was performed using a Shimadzu UV-2600 UV–Vis spectrophotometer. Field-emission scanning electron microscopy (SEM) observations were carried out using a FEI Quanta 250F. A UV–Vis spectrophotometer (T6 New Century, Beijing Persee Co., Ltd.) was used to analyze the temporal change in the absorption spectrum.

Electrochemical Measurements

Photocurrent measurements were performed on an electrochemical system (CHI-770, Chenhua, China) using a three-electrode configuration comprising a Pt plate as counter electrode, Ag/AgCl reference electrode, and a working electrode prepared as follows: 10 mg sample was dispersed in solution containing 150 μL isopropyl alcohol, 850 μL deionized water, and 30 μL naphthol. After ultrasonic treatment for 30 min, FTO glass (1 cm × 2 cm) as a support was covered with the suspension, then dried at 180°C under vacuum. All tests were carried out in 0.5 M Na_2SO_4 solution purged with nitrogen.

Photocatalytic Tests

In all experiments on catalytic performance, as-prepared photocatalyst (0.05 g) was added into a solution of RhB dye (100 mL, 10 mg/L). A 300-W Xe arc lamp equipped with an ultraviolet cutoff filter to provide visible light with $\lambda \geq 400$ nm was adopted as the visible-light source. Before irradiation, solutions with suspended photocatalyst were stirred magnetically in the dark for 60 min to achieve adsorption–desorption equilibrium. During irradiation, samples were collected at regular time intervals. The absorbance of RhB was monitored by UV–Vis spectroscopy (UV-2500PC, Shimadzu) at wavelength of 553 nm. Before spectroscopy measurements, the photocatalyst was removed by centrifugation.

The photocatalytic performance was also evaluated by photocatalytic oxidation (PCO) of NO at ppm level, which was stored in a cylindrical reactor and transported continuously. Photocatalyst (0.2 g) was placed on a small piece of clean cotton and strainer to prevent loss of the powder. The 300-W Xe arc lamp was used to provide light with $\lambda \geq 400$ nm, placed above the pipe (Supplementary Fig. S1). The gases (500 ppm NO, 7% O_2/N_2 balance) were supplied into the reactor at rate of 100 mL/min. Meanwhile, 30% H_2O_2 solution was dropwise added into the reactor using a pump at a slow rate of 0.08 mL/min. An NO_x analyzer (Sensonic IR-1) was used to detect the concentration of NO. The NO conversion was calculated using the formula

$$\text{NO conversion} = (NO_{in} - NO_{out})/NO_{in} \times 100\%.$$

RESULTS AND DISCUSSION

Structure and Morphology Characterization

X-ray powder diffraction (XRD) patterns were measured to investigate the phase structure of the as-prepared Bi_2WO_6. As shown in Fig. 1, all the peaks of BW could be mapped to orthorhombic Bi_2WO_6 in Joint Committee on Powder Diffraction Standards (JCPDS) card no. 73-1126. The peaks of BWR at 28.35°, 32.90°, 47.06°, 55.91°, and 58.62° were indexed to (131), (200), (202), (331), and (262) crystal planes of orthorhombic Bi_2WO_6, respectively, with no other impurity phases being found, indicating formation of pure single-phase Bi_2WO_6. Compared with BW, the broadened diffraction peaks of BWR indicated that the size of the crystallites was small. This is beneficial to enhance the

photocatalytic activity because small grain size generally means high specific surface area and more active sites.[25]

Morphology

The microstructure of the BWR product was determined by SEM (Fig. 2a). The BWR showed a novel rose-like hierarchical superstructure with average particle size of approximate 5.5 μm. Figure 2b shows a high-magnification SEM image of an individual Bi_2WO_6 hierarchical structure. Further observations clearly showed that the prepared BWR was built from numerous 2D nanoplates. These thin anisotropically directed nanoplates assembled into rose-like microstructures in a sequential and ordered manner. This specific 3D hierarchical frame is ideal for collecting photon energy and introducing reactive molecules into the internal space of the BWR, changing its optical absorption properties.[26] Such a hierarchical structure is also advantageous to increase diffusive transport of photoinduced holes to oxidize species, and facilitates separation of e^-–h^+ pairs during the photochemical reaction.[27] In addition, due to local supersaturation, tiny nanoparticles were also present on the edge of the nanoplates, as clearly revealed by imaging the edge of flowers. Meanwhile, the unique intercalation provides higher surface area and tremendous porous structure. The advantage of such porous features for improving pollution adsorption was further indicated by the RhB adsorption measurements (Table I). In addition, the presence of pores could provide more active sites and improve charge transfer to enhance the photocatalytic redox reaction.[28,29]

Based on these results, a possible mechanism for the formation of the rose-like BWR is proposed in

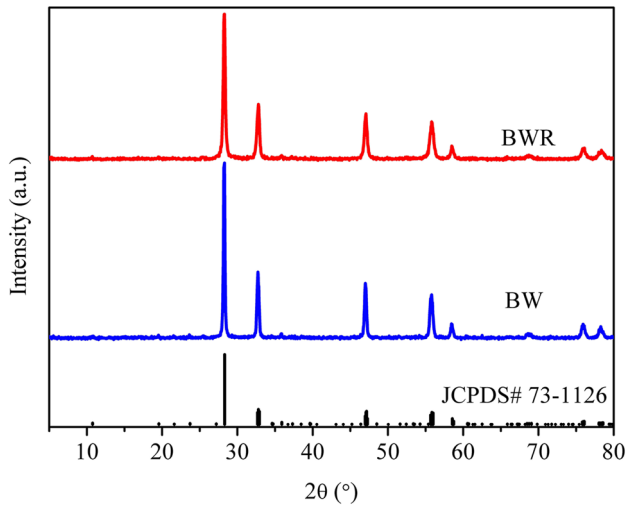

Fig. 1. XRD patterns of BW and BWR photocatalysts.

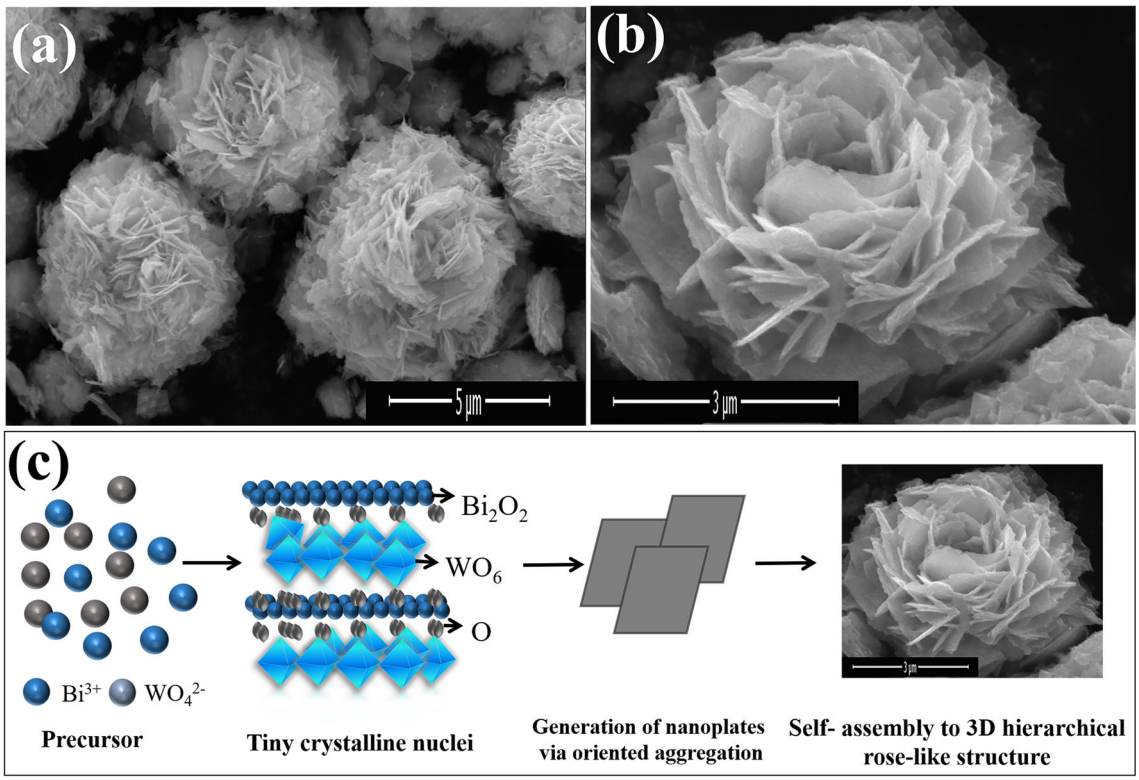

Fig. 2. (a, b) SEM images of BWR, (c) schematic illustration of proposed formation mechanism of 3D flower-like BWR superstructure.

Fig. 2c. Briefly, before hydrothermal treatment, WO_4^{2-} ions would react with Bi^{3+} ions to form amorphous Bi_2WO_6 nanoparticles by a precipitation process. The building blocks of the hierarchical superstructure were then produced from these aggregated nanoparticles through dissolution and recrystallization in the subsequent hydrothermal process.[23] At high temperature, these subunits would become curved and may stack or connect with each other. Subsequently, the mesoporous rose-like BWR superstructures formed.

BET Surface Area

In general, the specific surface area is a significant factor during photocatalytic processes, so BET measurements were carried out to evaluate the specific surface area of the obtained samples. As listed in Table I, the specific surface area of BWR was calculated to be 13.68 m^2/g, two times that of the irregular BW (7.35 m^2/g). This result indicates that higher specific surface area can be obtained by forming such 3D hierarchical structure. Generally, a catalyst with high surface area exhibits strong absorption ability. As shown by the results presented in Table I, the BWR superstructure with higher BET surface area could adsorb RhB molecules more efficiently compared with BW.

Optical Absorption Properties and Separation and Transfer of Charge Carriers

UV–Vis spectrometry was used to study the optical absorption spectrum of Bi_2WO_6 (Fig. 3), clearly revealing that BW exhibited light absorption properties between the ultraviolet and visible-light region. The impressive absorption exhibited by BW can be ascribed to the intrinsic bandgap of Bi_2WO_6. Compared with irregular BW, the absorption spectrum of BWR exhibited a slight red-shift, which would result in enhanced light harvesting. For a semiconductor, the bandgap can be estimated using the equation $ahv = A(hv - E_g)^{n/2}$, where a, n, A, h, and E_g are the absorption coefficient, light frequency, proportionality coefficient, Planck constant, and bandgap energy, respectively.[30] The value of n for $B_{i2}WO_6$ is 1.[31–33] According to the value of the intercept of $(ahv/A)^2$ and the tangent of the photon energy (hv) in Fig. 3b, the bandgap of irregular BW was found to be 2.79 eV, similar to previous reports.[25,34] However, the value for BWR decreased to 2.62 eV. The reason is that the unique hierarchical superstructure can cause multiple scattering of ultraviolet–visible light, thus increasing the optical path length through the hierarchical structure and thereby the light absorption, resulting in a narrower bandgap. Therefore, it is found that the morphology may have an important effect on the optical absorption properties of the samples.

The separation and transfer of charges play an important role in the photocatalytic process.[35,36] Electrochemical measurements are always used to evaluate the transfer efficiency of photogenerated charge carriers. The transient photocurrent responses (Fig. 4a) of the BW and BWR catalysts revealed that the photocurrent responded quickly when the light was switched on or off. It was clearly

Table I. BET surface area and RhB adsorption percentage over each catalyst in the dark

Sample	Surface area (m^2/g)	Pore volume (cm^3/g)	Adsorption (%)
BW	7.35	0.047	13
BWR	13.68	0.032	18

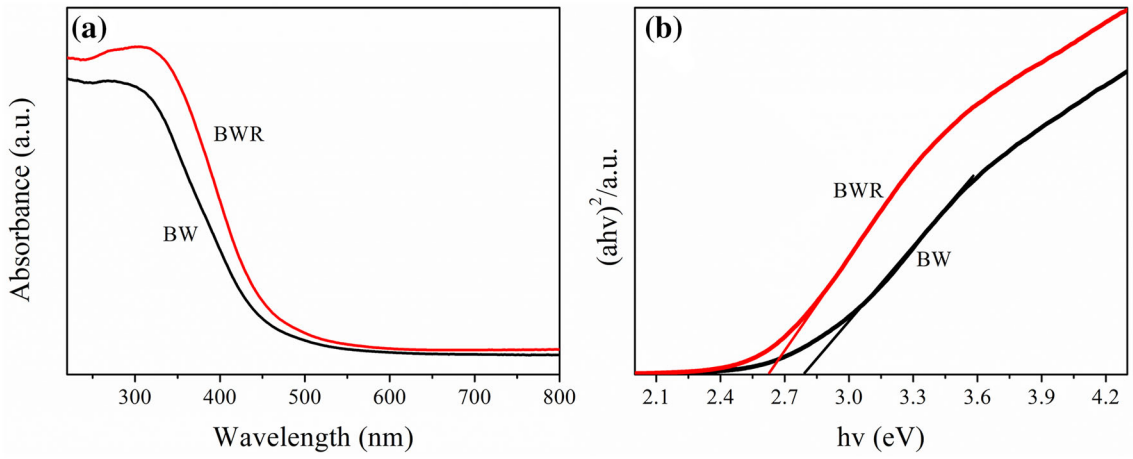

Fig. 3. UV–Vis absorption spectra (a) and plots of $(ahv/A)^2$ versus photon energy (b) of as-synthesized BW and BWR photocatalysts.

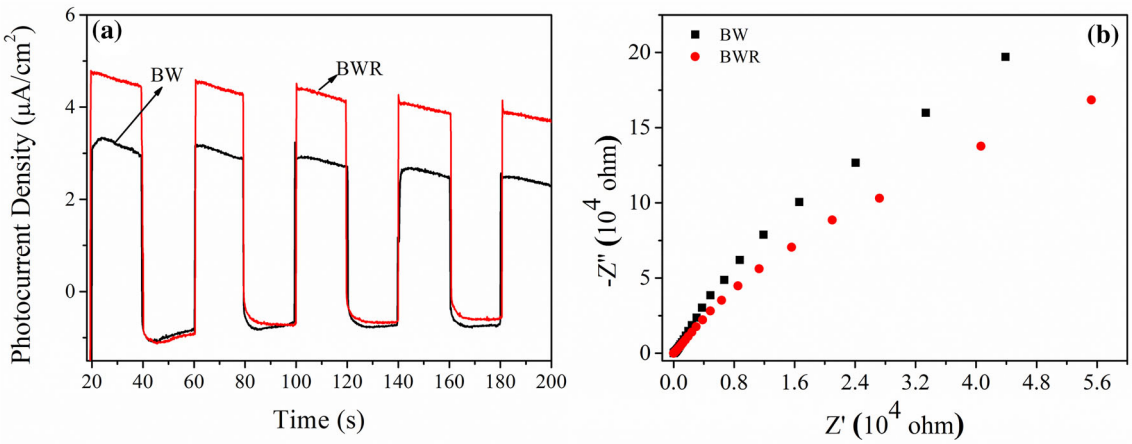

Fig. 4. (a) Photocurrent response versus time curves; (b) Nyquist plots of electrodes composed of BW and BWR samples.

observed that the BWR catalyst exhibited a higher photocurrent density, indicating extremely fast transfer of photoinduced charge carriers. To further clarify this result, electrochemical impedance spectroscopy (EIS) was applied. As shown by the Nyquist plots in Fig. 4b, compared with the BW sample, the arc radius for BWR was smaller, implying lower electron transfer resistance and more effective electron transfer. According to these results of the photocurrent response and EIS, it can be concluded that the BWR catalyst exhibited greater separation and migration efficiency of photogenerated e^-–h^+ pairs. Such fast separation and migration can be ascribed to interfacial effects among the hierarchical units of its 3D flower-like structure. In addition, the hierarchical structure increased diffusive transport of photoinduced holes to oxidize species, thus facilitating separation of e^-–h^+ pairs during the photochemical reaction.[27]

Photocatalytic Activities

The results of the photodegradation experiments on RhB using the different photocatalysts under visible-light irradiation are shown in Fig. 5. For comparison, a blank test without any photocatalyst was also carried out. The decrease in the concentration of RhB without photocatalyst was extremely slight (about 6%) under visible-light irradiation, demonstrating that RhB is stable and resists self-degradation. However, the degradation efficiency of RhB (98%) over BWR increased remarkably in comparison with BW (80%) in 120 min. This major improvement in the photocatalytic performance of BWR can be attributed to the enhanced adsorption, fast separation of photogenerated charge carriers, and narrower bandgap compared with irregular BW. Based on the adsorption spectra of RhB over BW and BWR after 60 min of adsorption–desorption equilibrium in the dark (Fig. 5b), BWR exhibited higher adsorption of RhB compared with BW, indicating a larger surface area. Figure 5c, d further shows the temporal evolution of the absorption spectra of the RhB in the presence of BW and BWR under visible-light irradiation. The absorption peak with BWR was smaller than that with BW at the same time interval. This result can be related to the hierarchical microstructure of BWR and indicates that tailoring the morphology represents a simple method to enhance efficiently the photocatalytic performance of a photocatalyst.

Mechanism Analysis

Several reactive species (·OH, h^+, and $\cdot O_2^-$) are potentially involved in the photocatalytic process. To further investigate the role of the main active substances during the photocatalytic degradation of RhB, trapping experiments were conducted on the BWR photocatalysts using five groups (I–V) of five quartz tubes containing 50 mL RhB and 0.2 mL 30% H_2O_2 solution. Among these, 30 mg BWR was added to groups II–V, respectively. Then, isopropyl alcohol (IPA) as ·OH scavenger, triethanolamine (TEOA) as h^+ scavenger, and *p*-benzoquinone (BQ) as $\cdot O_2^-$ scavenger.[37–40] were put into the tubes in groups III, IV, and V, respectively. Before irradiation, the solutions with catalysts were stirred without any light for 60 min to achieve adsorption–desorption equilibrium between the photocatalyst and RhB. Finally, all the quartz tubes were irradiated by visible light for 100 min with stirring. The photocatalyst in solution was removed by centrifugation, and the clear solution was investigated by UV–Vis spectroscopy at wavelength of 553 nm. Figure 6 shows the photocatalytic degradation performance of RhB solution over BWR under simulated visible-light irradiation in the absence or presence of each scavenger. Compared with in the absence of scavengers, note that all the scavengers suppressed the photocatalytic performance. The degradation efficiency of RhB was only

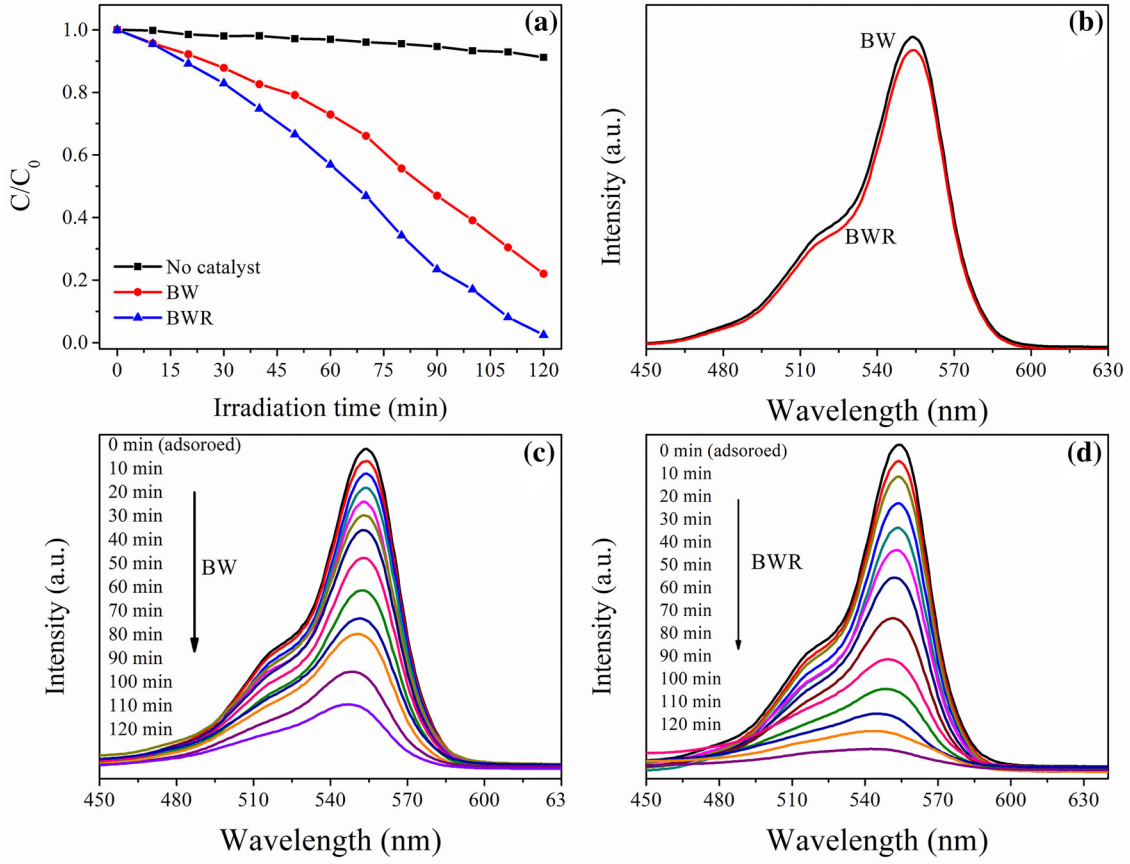

Fig. 5. (a) Degradation over samples of RhB under visible-light irradiation ($\lambda > 400$ nm) after different irradiation times; (b) absorption spectra of RhB in the dark for 30 min; (c, d) temporal evolution of UV–Vis spectrum of RhB at different irradiation times in presence of BW and BWR.

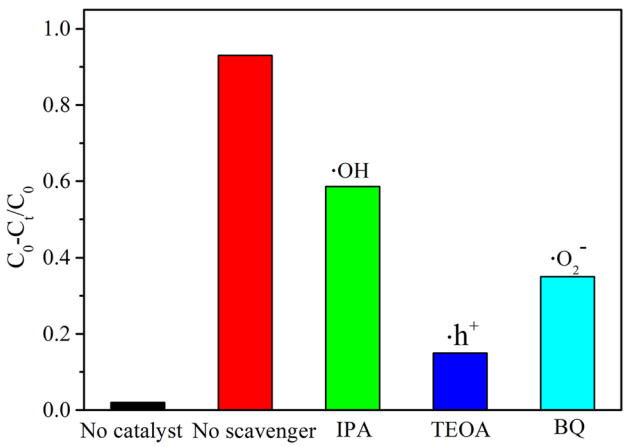

Fig. 6. Trapping experiments of active species over BWR during photocatalytic degradation of RhB.

5.5% within 100 min of irradiation without any photocatalyst. In the absence of scavengers, the photocatalytic efficiency of BWR was 91% within 100 min. With addition of 1 mM IPA solution, the degradation efficiency of RhB (58.1%) was partially inhibited. However, when 1 mM TEOA solution was added to the system, the degradation efficiency of RhB (9.2%) was almost completely inhibited, demonstrating that h^+ is the dominant active substance in this photodegradation process. Meanwhile, the BQ group also clearly exhibited reduced photodegradation of RhB (30.7%), indicating that the role of $\cdot O_2^-$ was greater than that of ·OH in the photocatalytic process of RhB. These experimental results show that the photodegradation efficiency decreased in the order IPA < BQ < TEOA. Thus, we can conclude that h^+ radicals were the dominant oxidative substance during the photocatalytic process.

Photocatalytic Activity

To investigate the scope of the obtained photocatalyst, the PCO performance of NO was also tested. The curves of PCO performance in Fig. 7a show that the PCO activity of NO without photocatalyst was negligible (6%). As the irradiation time was increased, it was observed that the photocatalytic efficiency of all the samples increased, finally becoming stable. At the start of the reaction, time is needed to produce the maximum amount of active species on the surface of the samples, resulting in the increasing trend in the PCO reaction.

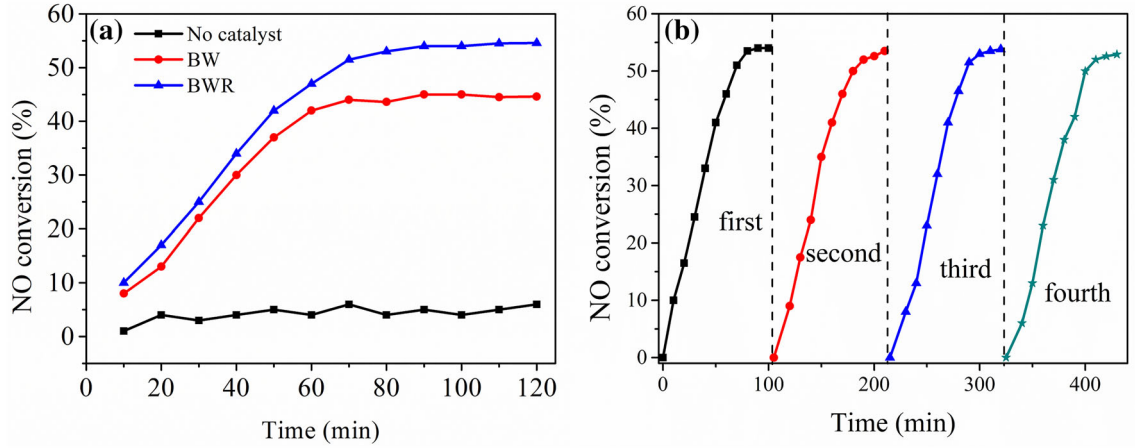

Fig. 7. (a) Photocatalytic oxidation of NO over BW and BWR and blank test; (b) stability of BWR sample for PCO of NO.

Obviously, the photocatalytic activity gradually improved, and the activity of the BWR sample increased to 54%, compared with 45% for BW. This enhanced photocatalytic activity might be contributed by the formation of the 3D superstructure, which provides high surface area for adsorption of target species, many active sites exposed on the surface of the catalyst, and improved transfer of charge carriers. Taking BWR as an instance, the photooxidation products of NO were detected by ion chromatography (Supplementary Fig. S2), but only NO_3^- could be detected in solution by qualitative analysis, indicating that the main reaction product of PCO of NO was NO_3^-. In addition, cyclic stability testing of PCO of NO over BWR catalyst was carried out. The results showed that about 53% PCO efficiency was retained after five cycles (Fig. 7b), indicating that the BWR catalyst exhibited superior recyclability.

CONCLUSION

Novel hierarchical rose-like Bi_2WO_6 assembled from nanoplatelets was successfully fabricated by a simple hydrothermal process. Compared with BW, the self-assembled BWR showed better photocatalytic performance under visible-light irradiation for PCO of NO and photodegradation of RhB, which can be ascribed to its narrower bandgap, higher surface area, and higher separation efficiency of photogenerated e^- and h^+ benefiting from the unique morphology. Further investigations showed that h^+ was the predominant active species. Furthermore, the results of this fundamental study not only exhibit this new morphology of Bi_2WO_6 but also provide insight into the facile design and fabrication of other novel hierarchical photocatalysts with high photocatalytic performance, having great potential applications in energy conversion or water and air treatment.

ACKNOWLEDGEMENTS

This work was financially supported by the Key Project of Chinese National Programs for Research and Development (2016YFC0203800), the National Natural Science Foundation of China (51578288), Industry–Academia Cooperation Innovation Fund Projects of Jiangsu Province (BY2016004-09), Jiangsu Province Scientific and Technological Achievements into a Special Fund Project (BA2015062, BA2016055 and BA2017095), and Top-notch Academic Programs Project of Jiangsu Higher Education Institutions, Postgraduate Research & Practice Innovation Program of Jiangsu Province (KYCX18_0446).

CONFLICT OF INTEREST

The authors declare that they have no conflicts of interest.

ELECTRONIC SUPPLEMENTARY MATERIAL

The online version of this article (https://doi.org/10.1007/s11837-019-03438-3) contains supplementary material, which is available to authorized users.

REFERENCES

1. Z. Jing, X. Qian, F. Zhaochi, L. Meijun, and L. Can, *Angew. Chem. Int. Ed.* 47, 1766 (2008).
2. F. Meng, Z. Hong, J. Arndt, M. Li, M. Zhi, F. Yang, and N. Wu, *Nano Res.* 5, 213 (2012).
3. N. Serpone, D. Lawless, and R. Khairutdinov, *J. Phys. Chem. C* 99, 16646 (1995).
4. A. Wold and A. Wold, *Chem. Mater.* 5, 280 (1993).

5. J. Low, S. Qiu, D. Xu, C. Jiang, and B. Cheng, *Appl. Surf. Sci.* 434, 423 (2018).
6. K. Hashimoto, H. Irie, and A. Fujishima, *Jpn. J. Appl. Phys.* 44, 8269 (2005).
7. T. Meißner, F. Eisenbeiß, and B. Jastorff, *Science* 293, 269 (2001).
8. H. Bai, K.S.Y. Kwan, Z. Liu, X. Song, S.S. Lee, and D.D. Sun, *Appl. Catal. B* 129, 294 (2013).
9. M. Zhu, C. Zhai, L. Qiu, L. Cheng, A.S. Paton, Y. Du, and M.C. Goh, *ACS Sustain. Chem.* 3, 3123 (2015).
10. N.A. Mcdowell, K.S. Knight, and L. Philip, *Chem. Eur. J.* 12, 1493 (2010).
11. H.W. Newkirk, P. Quadflieg, J. Liebertz, and A. Kockel, *Ferroelectrics* 4, 51 (1972).
12. F. Hongbo, P. Chengshi, Y. Wenqing, and Z. Yongfa, *J. Phys. Chem. B* 109, 22432 (2005).
13. H. Fu, C. Pan, W. Yao, and Y. Zhu, *J. Phys. Chem. B* 109, 22432 (2005).
14. Y. Shi, S. Feng, and C. Cao, *Mater. Lett.* 44, 215 (2000).
15. W. Chunying, Z. Hao, L. Fang, and Z. Lingyan, *Environ. Sci. Technol.* 44, 6843 (2010).
16. D. Xiao-Jun, L. Yong-Song, Z. Wei-Dong, and F. Shao-Yun, *Dalton Trans.* 39, 3426 (2010).
17. P. Sungho, L. Jung-Hyurk, C. Sung-Wook, and C.A. Mirkin, *Science* 303, 348 (2004).
18. Z. Tierui, D. Wenjun, K.-B. Mary, K. Sanjit, N. Roland, and T.Z. Ryan, *J. Am. Chem. Soc.* 128, 10960 (2006).
19. T. Hua, O. Shuxin, B. Yingpu, U. Naoto, O. Mitsutake, and Y. Jinhua, *Adv. Mater.* 24, 229 (2012).
20. J. Yu, J. Xiong, B. Cheng, Y. Yu, and J. Wang, *J. Solid State Chem.* 178, 1968 (2005).
21. S. Zhang, *J. Solid State Chem.* 179, 62 (2006).
22. J. Wu‡, F. Duan, Y. Zheng, and Y. Xie, *J. Phys. Chem. C* 111, 12866 (2007).
23. L. Zhang, W. Wang, Z. Chen, L. Zhou, H. Xu, and W. Zhu, *J. Mater. Chem.* 17, 2526 (2007).
24. C.S. Xu, F.Z. Yi, M. Rong, Y.Z. Yao, and Y.Y. Hao, *J. Hazard. Mater.* 192, 186 (2011).
25. C.Z. And and Y. Zhu, *Chem. Mater.* 17, 3537 (2005).
26. F. Dong, W. Zhao, Z. Wu, and S. Guo, *J. Hazard. Mater.* 162, 763 (2008).
27. P. Jong Hyeok, K. Sungwook, and A.J. Bard, *Nano Lett.* 6, 24 (2006).
28. J.G. Yu, Y.R. Su, and B. Cheng, *Adv. Funct. Mater.* 17, 1984 (2010).
29. W. Xinchen, J.C. Yu, H. Chunman, H. Yidong, and F. Xianzhi, *Langmuir* 21, 2552 (2005).
30. M.A. Butler, *J. Appl. Phys.* 48, 1914 (1977).
31. Y. Bian, W. Zeng, M. He, Y. Ma, Y. Liu, Y. Kong, and J. Pan, *J. Colloid Interface Sci.* 534, 20 (2019).
32. H. Zhou, Z. Wen, J. Liu, J. Ke, X. Duan, and S. Wang, *Appl. Catal. B* 242, 76 (2019).
33. Y. Liu, B. Wei, L. Xu, H. Gao, and M. Zhang, *ChemCatChem* 7, 4076 (2015).
34. S.O. Alfaro and M.D.L. Cruz, *Appl. Catal. A* 383, 128 (2010).
35. S. Zeng, P. Kar, U.K. Thakur, and K. Shankar, *Nanotechnology* 29, 052001 (2018).
36. H. Cheng, B. Huang, Y. Liu, Z. Wang, X. Qin, X. Zhang, and Y. Dai, *Chem. Commun.* 48, 9729 (2012).
37. Z.A. Huang, Q. Sun, K. Lv, Z. Zhang, M. Li, and B. Li, *Appl. Catal. B* 164, 420 (2015).
38. G. Jiang, Z. Wei, H. Chen, X. Du, L. Li, Y. Liu, Q. Huang, and W. Chen, *RSC Adv.* 5, 30433 (2015).
39. C. Tang, E. Liu, J. Wan, X. Hu, and J. Fan, *Appl. Catal. B* 181, 707 (2016).
40. C. Li, G. Chen, J. Sun, J. Rao, Z. Han, Y. Hu, W. Xing, and C. Zhang, *Appl. Catal. B* 188, 39 (2016).